J. Electroanal. Chem., 324 (1992) 229–242
Elsevier Sequoia S.A., Lausanne
JEC 01890

Microstructural and morphological changes induced in glassy carbon electrodes by laser irradiation

Nicholas M. Pontikos and Richard L. McCreery *
Department of Chemistry, The Ohio State University, 120 West 18th Ave., Columbus, OH 43210 (USA)
(Received 26 July 1991; in revised form 9 October 1991)

Abstract

Raman spectra, phenanthrenequinone adsorption, differential capacitance and scanning electron micrographs on fractured and polished glassy carbon (GC) surfaces were monitored before and after pulsed laser irradiation of varying power density. At power densities below 30 MW/cm^2, the Raman spectra, Γ_{PQ}, C°_{dl} and SEM appearance of polished surfaces changed slightly with laser activation. However, the Raman spectra of fractured GC indicated increased disorder during laser irradiation. After vigorous laser treatment, the Raman spectrum became similar to that of the polished surface, but Γ_{PQ} and C°_{dl} on the fractured surface did not change greatly at power densities below 30 MW/cm^2. At higher power densities, both polished and fractured surfaces showed significantly higher Γ_{PQ} and C°_{dl}, and the SEMs showed evidence of local melting. After 70 MW/cm^2 laser treatment, the fractured and polished surfaces were quite similar. The results support a mechanism based on thermomechanical shock below about 30 MW/cm^2 and local melting above this threshold.

INTRODUCTION

The selection of an appropriate carbon material for a specific electrochemical application is complicated due to the difficulty in predicting its electrochemical behavior, specifically the heterogeneous electron transfer rate constant k° [1,2]. A significant body of literature has been devoted to the explanation of the many factors which affect k° on a variety of carbon surfaces, with glassy carbon being the most widely studied carbon material in the context of electrode kinetics [2–11]. The use of glassy carbon (GC) as an electrode material is widespread due to its wide potential range, relatively low cost, low porosity, chemical inertness, and availability. However, electrochemical applications of GC are complicated by the

* To whom correspondence should be addressed.

fact that its behavior is highly dependent on its surface history. The mechanisms of pretreatment procedures for GC activation toward electron transfer and the subsequent passivation during use are not completely understood.

Several surface pretreatment procedures have been developed for enhancing k° on glassy carbon. They include polishing [5,6], chemical and electrochemical pretreatment [12–15], vacuum heat treatment [7,16], thermal and rf plasma treatments [7,8,17,18], and laser activation [3,10,11,19]. These methods produce carbon surfaces which show increases in k° by factors of 10 to 1000 relative to conventionally polished surfaces for benchmark systems such as $Fe(CN)_6^{3-/4-}$ [1,5]. The mechanism of these increases in k° remains an active area of research. Kuwana et al. and Wightman et al., proposed that active sites exist on carbon and that the removal of impurities such as polishing debris and surface oxygen expose these sites [5,7,20–22], while others propose that oxygen functionalities enhance k° for certain redox systems [15,23]. Considering the problem generally, the determination of which surface variables affect GC electrode behavior is complex because several electrochemical observations are affected by more than one independent surface variable. For example, k°, capacitance, and adsorption each depend on the independent variables of surface roughness, surface edge plane density, and surface coverage of oxides or impurities. Since pretreatment procedures such as polishing and electrochemical pretreatment affect more than one independent surface variable, the mechanism of activation is difficult to determine.

In several previous reports, the number of surface variables was reduced by starting with the basal plane of highly ordered pyrolytic graphite (HOPG) [24–26]. For this case, it was concluded that k° for $Fe(CN)_6^{3-/4-}$ was much larger on graphitic edge plane than on basal plane, and the observed k° was determined primarily by the fractional coverage of edge plane on the surface. A subsequent study of GC also sought to reduce the number of surface variables by examining k° on a GC surface created by fracturing in the electrolyte solution. This surface did not undergo any intentional pretreatment, yet exhibited a high (0.5 cm/s) k° for $Fe(CN)_6^{3-/4-}$ in 1 M KCl [3]. In the current investigation, the fractured GC surface was examined in more detail, and compared with a conventionally polished surface. By observing Raman spectra, phenanthrenequinone (PQ) adsorption, capacitance, and k°, we sought to gain a better understanding of GC surface variables which affect electrode kinetics.

EXPERIMENTAL

Raman spectra of GC surfaces were obtained in air with 514.5 nm light and a Spex 1403 spectrometer. The spectral bandpass was 10 cm^{-1}, and typical laser power at the sample was between 50 and 70 mW. Laser activation was performed using a Quantel (Continuum) model 580–10 Nd:YAG laser delivering 9 ns pulses at 1064 nm. Laser pulses were delivered in groups of three unless otherwise noted, in order to average spatial and temporal variations. Power density was determined by measuring the average power through a 1.4 mm metal aperture. The electro-

chemical cell used for all experiments was constructed of Teflon with a BK-7 quartz window (> 95% transmittance) to allow the 1064 nm laser radiation to impinge upon the GC-20 electrode in solution.

GC-20 working electrodes were fabricated from a Tokai GC-20 plate by first diamond sawing the carbon then sanding the piece obtained into a small rectangle of approximate dimensions $0.05 \times 0.05 \times 1.0$ cm. The carbon microrod was then mounted onto a conducting surface and coated with Eccobond Epoxy (Emerson & Cuming, Inc., Woburn, MA) as opposed to the Torr Seal (Varian) used previously [3]. Prior to each use, the glassy carbon electrode was polished with slurries of 1.0, 0.3, and 0.05 μm alumina in Nanopure (Barnstead, Boston, MA) water on microcloth (Buehler), then sonicated briefly to remove polishing debris. A Bioanalytical Systems (BAS) Ag/AgCl/3 M NaCl electrode was used as the reference, while a platinum wire served as the auxiliary electrode. Prior to fracturing, the Eccobond epoxy was filed away to expose a short GC "post", which was scored and fractured in solution such that the end of the post became the active surface. Typical areas, as measured by single step chronoamperometry of $Fe(CN)_6^{4-}$ in 1 M KCl, were on the order of 0.005 cm^2 for the exposed GC-20 face. These small electrodes were necessary in order to ensure a "mirror" region upon fracturing [3].

Electrochemical measurements were performed using customized computer software and a Scientific Solutions Labmaster analog interface board which controlled an Advanced Idea Mechanics model 18709 potentiostat (Columbus, OH). The potentiostat was driven by a triangular potential vs. time ramp from a Tektronix 501A function generator. Apparent capacitance was measured by the method of Gileadi [27,28] which involved applying a 100 Hz, 20 mV peak-to-peak triangle wave centered on 0.0 V vs. Ag/AgCl from the Tektronix function generator and recording the current response on a Lecroy 9400A digital oscilloscope. The area used in the calculation of capacitance and PQ adsorption was determined by chronoamperometry of $Fe(CN)_6^{4-}$ on a 1 to 5 s time scale. Background corrected current vs. $t^{-1/2}$ plots were linear.

Phenanthrenequinone (PQ) was recrystallized three times from benzene prior to use. The magnitude of PQ adsorption was determined by the method of Anson [29], using a 10^{-6} M solution in 1 M $HClO_4$. The area of the PQ reduction voltammetric peak above background (obtained at 100 mV/s) was used to determine the adsorbed charge, Q_{ad}, and Γ_{PQ} was calculated based on the chronoamperometric area.

RESULTS

Raman spectra of carbon have been examined previously and found to be quite sensitive to the microstructure of the sp^2 carbon material [1,3,30–32]. GC-20 has a strong 1360 cm^{-1} band which is negatively correlated with the size of the graphitic planes. This band becomes active due to a symmetry breakdown at the graphitic edges. Tuinstra and Koenig reported a linear correlation between the reciprocal of

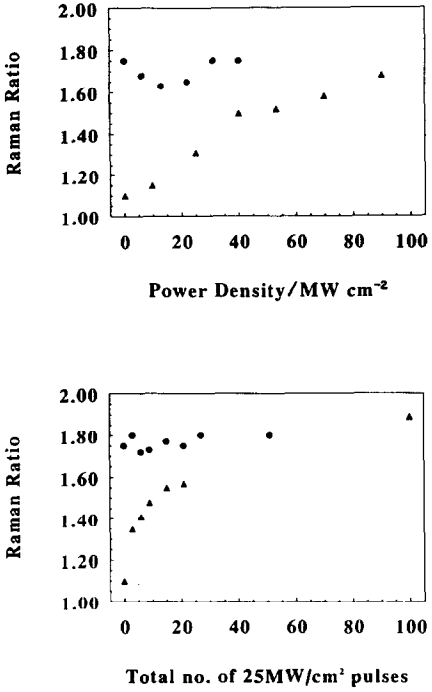

Fig. 1. Raman intensity ratio of GC-20 vs. power density (top) and successive 25 MW/cm^2 pulses (bottom). • Polished surfaces, (▲) fractured surfaces. For the top plot, a freshly fractured GC surface was used for each triangular point.

the microcrystallite size ($1/L_a$) and the 1360/1582 Raman intensity ratio, with larger ratios implying more graphitic edges and smaller microcrystallites [32]. For glassy carbon, we demonstrated that the 1360/1582 intensity ratio is sensitive to pretreatment procedures [3,30]. Specifically, fracturing a GC-20 microrod produces an intensity ratio of 1.1, while polishing increases this ratio to 1.8, implying mechanical generation of smaller microcrystallites.

A fractured surface was observed first since it is initially free of surface contaminants and presumably representative of the unmodified bulk GC. The top plot in Fig. 1 summarizes the results for varying power density. Each data point was obtained by starting with a freshly fractured GC surface, then exposing the surface to three laser pulses. The 1360/1582 Raman intensity ratio increases for a fractured surface with increasing Nd:YAG power density, indicating that microstructural changes are occurring. Although the intensity ratio starts at a higher value for the polished surface, it shows little change with laser activation, implying that no major additional microstructural changes are induced. The bottom graph in Fig. 1 shows polished and fractured surfaces exposed to successive 25 MW/ cm^2 Nd:YAG pulses. The pulses were delivered in groups of three followed by acquisition of Raman spectra with the sequence being repeated until 99 pulses had

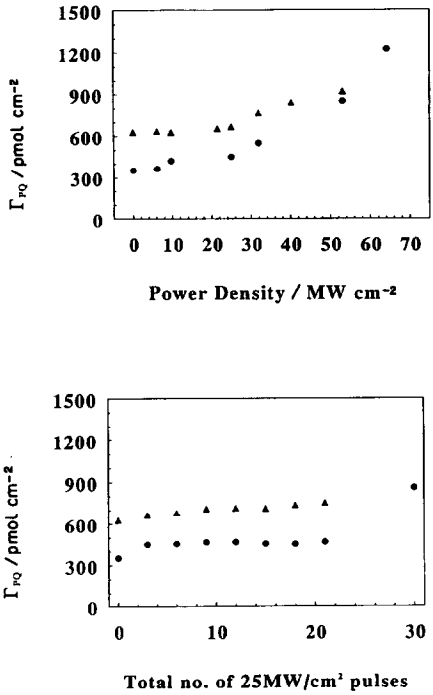

Fig. 2. Adsorption of phenanthrenequinone vs. power density (top) and successive 25 MW/cm^2 pulses (bottom). Electrodes were encapsulated in Eccobond epoxy. (●) Surfaces which were polished prior to laser irradiation, (▲) surfaces which were initially fractured.

been delivered. These results indicate that the Nd:YAG laser causes microstructural changes for a fractured surface, at least to a depth comparable to the Raman sampling depth of ca. 30 nm [33]. Apparently laser activation of a surface already modified by polishing has little further effect on the carbon microstructure, at least to any extent observable with Raman spectroscopy.

The effects of laser activation on phenanthrenequinone (PQ) adsorption and the differential capacitance of fractured and polished surfaces are shown in Figs. 2 and 3. Γ_{PQ} (pmol/cm^2) was determined voltammetrically via the equation

$$Q_{ads} = nFA_g\Gamma_{PQ} \tag{1}$$

where Q_{ads} is the integral of the background corrected voltammetric peak for adsorbed PQ, n is 2, F is the Faraday constant, A_g is the chronoamperometric area, and Γ_{PQ} is the equilibrium coverage of PQ. Note that Γ_{PQ} is based on chronoamperometric area and makes no presumptions about microscopic area. The differential capacitance was determined via the equation

$$I_{p-p} = 2\nu A_g C_{dl}^{\circ} \tag{2}$$

where I_{p-p} is the peak-to-peak current due to double layer charging in response to an imposed 20 mV p – p triangle wave, ν is the slope of the triangle wave, A_g is chronoamperometric area, and $C°_{dl}$ is the double layer capacitance (μF/cm^2).

Referring first to Fig. 2, it is apparent that Γ_{PQ} increases slightly with laser irradiation below 25 MW/cm^2 for either polished or fractured surfaces. Note that Γ_{PQ} starts at ca. 600 pmol/cm^2 for the fractured surface, about twice the value on the polished surface. For repetitive 25 MW/cm^2 pulses, Γ_{PQ} on either surface increases by at most 40% over initial values. In addition, the fractured surface exhibits consistently higher Γ_{PQ} for all conditions except high power densities. Γ_{PQ} for both fractured and polished GC increases significantly with laser activation, by more than a factor of 3 for polished GC at high power density. The Γ_{PQ} values reported here are significantly higher than those reported previously [3] for GC encapsulated in Torr-seal epoxy. We attribute this difference to reduced contamination of the surface by the Eccobond epoxy compared to Torr-seal, for several reasons. Γ_{PQ} was comparable to the Eccobond values when the GC was encapsulated in compression molded Kel-F prior to fracturing. Dopamine adsorption on fractured GC decreased with time after fracture for Torr-seal encapsulation, but was much more stable for Eccobond [34]. It is possible that the seal between Eccobond and GC is prone to microcracks, increasing the effective adsorption area. However, this possibility is quite unlikely. Optical microscopy of the Eccobond/GC seal revealed no cracks, and Γ_{PQ} was quite reproducible. As noted below, fast cyclic voltammograms of $Fe(CN)_6^{3-/4-}$ had the expected shape for planar diffusion without any cracks. Finally, large cracks are ruled out by the good agreement between the geometric and chronoamperometric areas.

Similar behavior was observed for capacitance, shown in Fig. 3. At 25 MW/cm^2 or below, capacitance is not affected greatly by laser irradiation, but the fractured surface always exhibits higher $C°_{dl}$ than the polished surface. In addition, repetitive 25 MW/cm^2 pulses increase capacitance by about 50%, as noted in a previous report [3]. Above 25 MW/cm^2, $C°_{dl}$ for the polished surface increases markedly. Although the $C°_{dl}$ values for the polished surface before and during laser activation are similar to those reported previously [3], the fractured $C°_{dl}$ values are somewhat higher (55 vs. 36 μF/cm^2), probably because of the difference in the encapsulation material mentioned earlier.

Scanning electron micrographs of polished and fractured surfaces are shown in Figs. 4 and 5, respectively. In all cases, the samples were gold coated before SEM. Micrographs obtained at lower magnification were featureless, and resembled images reported previously by Kazee et al. [35], and by our laboratory [10]. The fine structure apparent in Figs. 4 and 5 may not have been visible in previous work because the current samples were gold coated or because of differences in polishing procedures. The apparent fissures in Fig. 4a are discussed in more detail below. In Fig. 4b, following 40 MW/cm^2 laser activation, new features are observed which were not observed following 25 MW/cm^2 irradiation. After 70 MW/cm^2 the surface is characterized by occasional large defects (visible at the right) in a sea of small ($\sim$ 0.1 μm) nodules. Thus major morphological changes

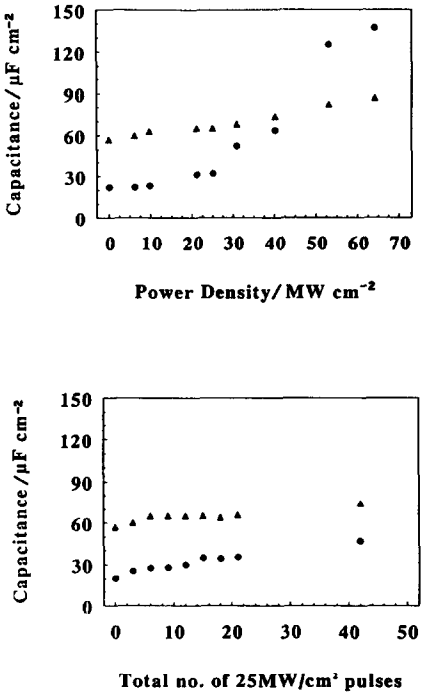

Fig. 3. Apparent capacitance vs. power density (top) and successive 25 MW/cm^2 pulses (bottom). (•) surfaces which were initially polished, (▲) surfaces which were initially fractured.

occurred to the polished surface between 25 and 70 MW/cm^2, starting below 40 MW/cm^2. The fractured surface of Fig. 5a exhibits nodules of GC distributed fairly homogeneously. No obvious changes are apparent upon laser activation at 40 MW/cm^2 (Fig. 5b) and 70 MW/cm^2 (Fig. 5c). Manual measurement of the nodules revealed an average diameter for the fractured surface of 0.16 ± 0.05 μm ($N = 109$), which decreased to 0.09 ± 0.03 μm ($N = 100$) upon 70 MW/cm^2 laser activation.

The SEMs appear to reveal microcracks on the polished surface, as well as small fissures between nodules on the fractured surface. It is reasonable to suspect that these apparent cracks will affect voltammetric peak shapes, since electroactive species in the cracks will undergo thin layer rather than semi-infinite diffusion. This possibility was tested by comparing voltammograms for $Fe(CN)_6^{3-/4-}$ (1 M KCl) at 100 V/s with simulated curves calculated assuming linear diffusion, with the results shown in Fig. 6. The background current decreased somewhat when the solution was changed from $Fe(CN)_6^{3-/4-}$ to blank electrolyte, so the background subtraction was not completely effective. Nevertheless, the voltammograms for both the fractured and 70 MW/cm^2 surfaces have shapes very close to that simulated for a k° of 0.4 cm/s. The predicted peak current for planar diffusion is

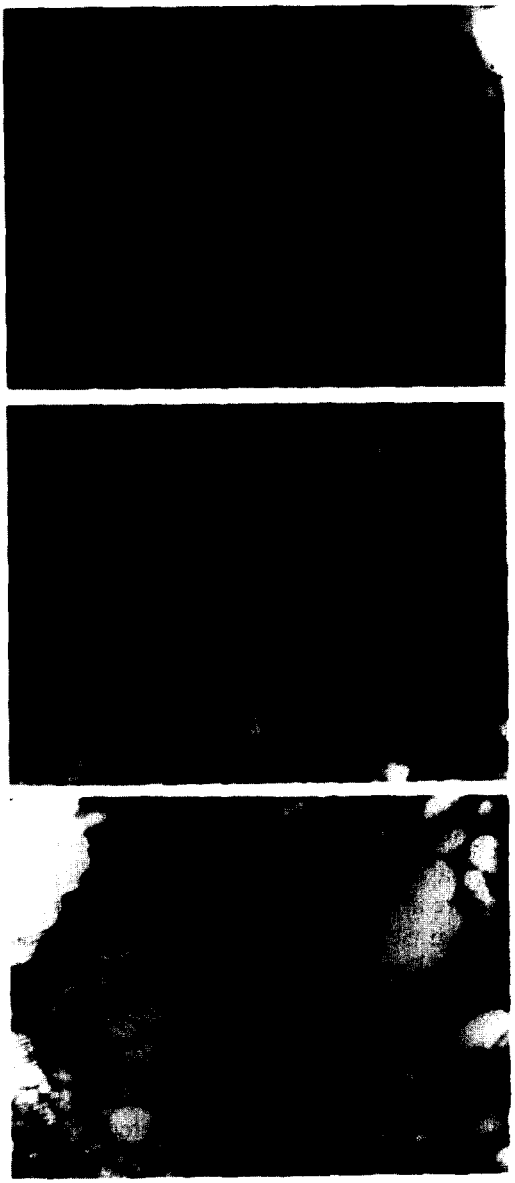

Fig. 4. Scanning electron micrographs of polished and laser irradiated GC-20 surfaces. (a) Freshly polished, (b) polished + three 40 MW/cm^2 Nd:YAG pulses, (c) polished + three 70 MW/cm^2 Nd:YAG pulses.

32 μA for the conditions of Fig. 6a, and the observed value is 35 μA. Thus the apparent microcracks or nodules did not cause an observable deviation from planar electrode behavior. In addition, semi-integration of either voltammogram in

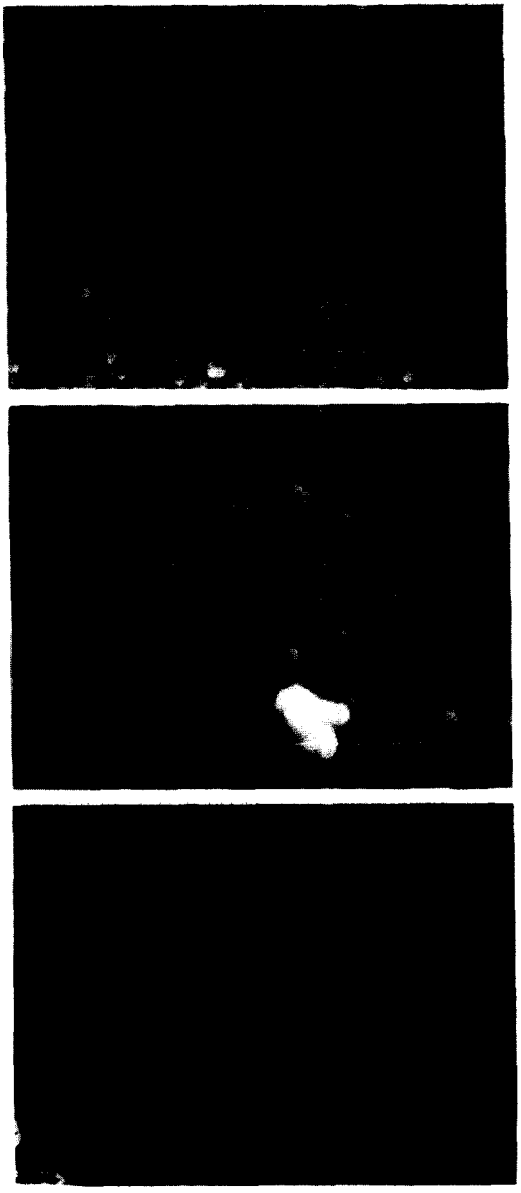

Fig. 5. Scanning electron micrographs of fractured and laser irradiated GC-20 surfaces. (a) Fractured, (b) fractured + three 40 MW/cm^2 Nd:YAG pulses, (c) fractured + three 70 MW/cm^2 Nd:YAG pulses.

Fig. 6 yielded the expected sigmoidal shape [36], with no indication of adsorption or thin layer behavior. Both voltammetry and semi-integration are consistent with an SILD assumption for the conditions employed.

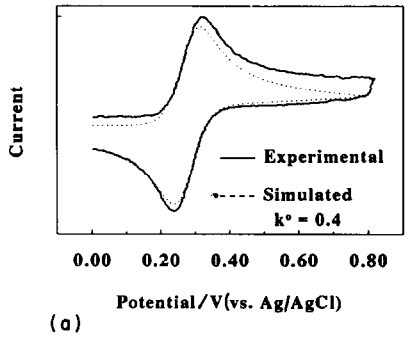

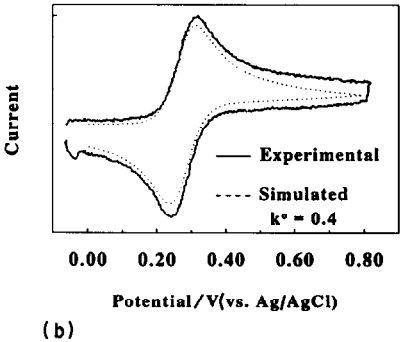

Fig. 6. Comparison of experimental (———) and simulated (- - - - -) voltammograms for $Fe(CN)_6^{3-/4-}$ in 1 M KCl, 100 V/s. Background on experimental curves resulted from incomplete background subtraction caused by a changing background current. (a) Fractured GC-20; (b) fractured + three 70 MW/cm^2 laser pulses. Simulated and experimental current scales were arbitrarily adjusted to be equal before comparison.

DISCUSSION

As noted earlier, a difficulty in relating carbon surface structure to reactivity is the separation of variables dealing with microstructure, roughness, and cleanliness. The common dependent variables such as $k°$, background current, and capacitance depend on more than one of the independent variables dealing with the surface, so one must attempt to monitor these surface variables with some other observables. The Raman intensity ratio of Fig. 1 is a good example, since the L_a and L_c microcrystallite sizes are in the region of 2.5–10.0 nm, and would not be expected to depend on surface cleanliness or roughness. Thus changes in Raman intensity ratio indicate primarily carbon microstructure with little interference from other variables. Figure 1 confirms that the microstructure of the polished surface is already altered from the fractured surface, and is not modified further by the laser. In contrast, the Raman ratio indicates a decrease in L_a with laser treatment of the fractured surface for either repetitive 25 MW/cm^2 pulses or increasing power

density. With extensive or high powered laser treatment, the Raman ratio for the fractured surface approaches that of the polished surface. Thus as far as carbon microstructure is concerned, the nature of the surface following extensive laser activation does not appear to depend on whether the surface was initially fractured or polished.

One would expect Γ_{PQ} to depend on both microscopic surface area and surface cleanliness. However, the fact that Γ_{PQ} does not increase greatly for laser activation in the 0–25 MW/cm^2 power density range implies that cleanliness is not a major factor affecting Γ_{PQ}. Since 25 MW/cm^2 laser pulses increase $k°$ for $Fe(CN)_6^{3-/4-}$ by at least two orders of magnitude for a polished surface, one would presume that the surface is cleaned significantly by the laser [30]. Apparently PQ adsorbs strongly enough that adsorbed impurities, at least those affected by the laser, have only minor effects on Γ_{PQ}. This argument leads to the conclusion that Γ_{PQ} is primarily a measure of surface roughness. Operating under this assumption, the results shown in Fig. 2 lead to two conclusions. First, surface roughness does not change greatly for up to twenty-one 25 MW/cm^2 laser pulses or up to ca. 30 MW/cm^2 power density. This conclusion is consistent with the SEM results, which show minor changes in surface morphology for these conditions. Second, the fractured surface has a higher roughness factor than the polished surface. In relative terms, the fractured surface has a microscopic area about 1.8 times the polished surface. On an absolute scale, the ideal monolayer coverage for PQ on a flat surface, based on Van der Waals radii, is 177 pmol/cm^2 [37]. Therefore the observed roughness factor for the polished surface is about 1.9, while for the fractured surface it is about 3.5. Laser irradiation above 30 MW/cm^2 increases the roughness factor significantly for both surfaces. It is obvious that the roughness factor is strongly dependent on surface preparation and history.

The changes in capacitance are similar to those in Γ_{PQ}, although one would expect $C°_{dl}$ to depend on additional surface variables such as oxides, electrolyte adsorption, etc. As with Γ_{PQ}, the initial $C°_{dl}$ for the fractured surface is about twice that of the polished surface. $C°_{dl}$ increases more rapidly during laser activation of the polished surface compared to the fractured surface, and this increase correlates with electron transfer activation. However, major increases in $C°_{dl}$ were not observed until laser powers of 30 MW/cm^2 and above were delivered.

The voltammetry of Fig. 6 indicates that any surface roughness or heterogeneity is small on the scale of a diffusion layer at 100 V/s. For the time required to scan from the foot of the reduction wave to its peak (1 ms), $\sqrt{Dt}$ is about 0.70 μm. Thus the approximate diffusion layer thickness is much greater than the surface structural features observable by SEM (0.1 μm), even at the fairly high scan rates employed. As a consequence, the microscopically rough surfaces of either polished or fractured GC do not affect planar diffusion significantly.

Based on electrochemical, Raman, and SEM results, a model of the GC surface may be formulated. As shown in Fig. 5a, the fractured GC surface consists of nodules with a mean diameter of 0.16 μm. These nodules are presumably present throughout the material, and were formed when the original GC was fabricated. In

work to be reported elsewhere, we have observed such nodules with scanning tunneling microscopy on fractured GC [38]. On the basis of Fig. 4A, the polishing process flattens the exposed hemisphere of each nodule to yield relatively flat structures. The cracks between nodules presumably contribute to the microscopic area, but are not large or deep enough to contribute to the observed voltammetry. Since the surface area of a hemisphere is twice the area of a circle with the same radius, an idealized case of closely packed hemispheres would have twice the microscopic area of a collection of closely packed circles, ignoring voids. This ideal case is clearly oversimplified, but it does demonstrate that a surface consisting of nodules has a larger microscopic area than a flat surface, by approximately the ratio observed for Γ_{PQ} and C_{dl}°.

Up to 25 MW/cm^2, laser irradiation has relatively minor effects on Γ_{PQ}, C_{dl}° and SEM appearance, but it does increase the Raman intensity ratio. On the basis of the intensity ratio, the a-axis microcrystallite size decreases from ca. 5.0 nm in the fractured case to roughly 2.5 nm upon laser activation [32]. Apparently this scale is too small to affect C_{dl}° or Γ_{PQ} significantly, since these electrochemical variables do not track the Raman ratio. The laser induced microstructural changes are presumably caused by thermally induced mechanical shock during the rapid heating accompanying laser activation. Thus at 25 MW/cm^2 and below, the results are consistent with a laser activation mechanism based on surface cleaning.

At 30 MW/cm^2 and above, obvious changes are apparent in the SEMs, C_{dl}° and Γ_{PQ}. In Fig. 4b (40 MW/cm^2) nodules are apparent, and in Fig. 4c (70 MW/cm^2) they are dominant. For the fractured surface, the nodules are apparent with or without laser treatment, but they do decrease in size upon 70 MW/cm^2 irradiation. Based on a simple model ignoring phase changes, we showed previously that 25 MW/cm^2 pulses will cause a maximum surface temperature excursion of about 3700 K, and that this excursion is linear in power density [39]. Since the melting point of graphite is estimated at 4300 K, laser pulses of 30 MW/cm^2 and higher power density should be able to melt the GC surface. Melting should distort the polished surface and possibly revert the surface back to nodules. For a fractured surface, melting and resolidifying causes no obvious structural changes, but does reduce nodule size. The main conclusion is that the changes in C_{dl}° and Γ_{PQ} starting at 30 MW/cm^2 are likely to be due to localized melting induced by the laser. Since power densities well below this melting threshold are adequate for activation of electron transfer, melting is probably not directly relevant to electron transfer activation. However, melting leads to obvious morphological and electrochemical changes, and is an important phenomenon for a general understanding of laser effects on carbon electrodes.

From an electroanalytical perspective, it is obvious that it is possible to overdo laser activation with high power densities, leading to high capacitive background and high microscopic area. On the other hand, laser treatment at 25 MW/cm^2 and below leads to major increases in k° without obvious surface structural changes [3,10] From a mechanistic standpoint, the results at 25 MW/cm^2 and below demonstrate that laser activation of k° does not require roughness or microstruc-

tural changes, and must involve a phenomenon not probed by Γ_{PQ}, Raman, or SEM, probably involving removal of surface impurities.

ACKNOWLEDGEMENTS

This work was funded by The Air Force Office of Scientific Research. The authors thank Christie Allred for development of the software to control the Lecroy oscilloscope and for useful discussions concerning this work. We also acknowledge preliminary experiments by Ronald Rice which indicated nodules on fractured GC, plus the valuable assistance of Clare McDonald in obtaining SEM images.

REFERENCES

1 K. Kinoshita, Carbon: Electrochemical and Physicochemical Properties, Wiley, New York, 1988.
2 R.L. McCreery, in A.J. Bard (Ed.), Electroanalytical Chemistry, Vol. 17, Marcel Dekker, New York, 1991, pp. 221–374.
3 R.J. Rice, N.M. Pontikos and R.L. McCreery, J. Am. Chem. Soc., 112 (1990) 4618.
4 R.N. Adams, Electrochemistry at Solid Electrodes, Marcel Dekker, New York, 1969.
5 I.F. Hu, D.H. Karweik and T. Kuwana, J. Electroanal. Chem., 188 (1985) 59.
6 G.N. Kamau, W.S. Willis and J.F. Rusling, Anal. Chem. 57 (1985) 545.
7 D.T. Fagan, I.F. Hu and T. Kuwana, Anal. Chem., 57 (1985) 2759.
8 R.M. Wightman, M.R. Deakin, P.M. Kocach, W.G. Kuhr and K. Stutts, J. Electrochem. Soc., 131 (1984) 1578.
9 L.J. Kepley and A.J. Bard, Anal. Chem., 60 (1988) 1459.
10 M. Poon and R.L. McCreery, Anal. Chem., 58 (1986) 2745.
11 M. Poon and R.L. McCreery, Anal. Chem., 59 (1987) 1615.
12 R.C. Engstrom, Anal. Chem., 54 (1982) 2310.
13 R.C. Engstrom and V.A. Strasser, Anal. Chem., 56 (1984) 136.
14 G.E. Cabaniss, A.A. Diamantis, W.R. Murry Jr., R.W. Linton and R.J. Meyer, J. Am. Chem. Soc., 107 (1985) 1845.
15 L. Falat and H.Y. Cheng, J. Electroanal. Chem., 157 (1983) 393.
16 R.M. Wightman, E.C. Park, S. Borman and M.A. Dayton, Anal. Chem., 50 (1978) 1410.
17 C.W. Miller, D. Karweik and T. Kuwana, Anal. Chem., 53 (1979) 2319.
18 J. Evans and T. Kuwana, Anal. Chem., 51 (1979) 358.
19 M. Poon and R.L. McCreery, Anal. Chem., 60 (1988) 1725.
20 K.J. Stutts, P.M. Kovach, W.G. Kuhr and R.M. Wightman, Anal. Chem., 55 (1983) 1632.
21 I.F. Hu and T. Kuwana, Anal. Chem., 58 (1986) 3235.
22 P.M. Kovach, M.R. Deakin and R.M. Wightman, J. Phys. Chem., 90 (1986) 4612.
23 J.F. Evans and T. Kuwana, Anal. Chem., 49 (1977) 1632.
24 I. Marcos and E. Yeager, Electrochim. Acta., 15 (1970) 953.
25 R. Bowling, R.T. Packard and R.L. McCreery, Langmuir, 5 (1989) 683.
26 R.J. Bowling, R.T. Packard and R.L. McCreery, J. Am. Chem. Soc., 11 (1989) 1217.
27 E. Gileadi and N. Tshernikovski, Electrochim. Acta., 16 (1971) 579.
28 E. Gileadi, N. Tshernikovski and M. Babai, J. Electrochem. Soc., 119 (1972) 1018.
29 A.P. Brown and F.C. Anson, Anal. Chem., 49 (1977) 1589.
30 R.J. Rice, C.D. Allred and R.L. McCreery, J. Electroanal. Chem., 263 (1989) 163.
31 M. Nakamizo and K. Tamai, Carbon, 22 (1984) 197.
32 F. Tuinstra and J.L. Koenig, J. Phys. Chem., 53 (1970) 1126.
33 Y.W. Alsmeyer and R.L. McCreery, Anal. Chem., 63 (1991) 1289.

34 C.D. Allred and R.L. McCreery, Anal. Chem., in press.
35 B. Kazee, D. Weisshaar and T. Kuwana, Anal. Chem., 57 (1985) 2736.
36 R. Bowling and R.L. McCreery, Anal. Chem., 60 (1988) 605.
37 M.P. Soriaga and A.T. Hubbard, J. Am. Chem. Soc., 104 (1982) 2735.
38 M.T. McDermott, C.D. Allred and R.L. McCreery, in preparation.
39 R.J. Rice and R.L. McCreery, J. Electroanal. Chem., 310 (1991) 127.